Clinical Neurophysiology 155 (2023) 44–54

Contents lists available at ScienceDirect

Clinical Neurophysiology

journal homepage: www.elsevier.com/locate/clinph

Monopolar tDCS might affect brainstem reflexes: A computational and neurophysiological study

Matteo Guidetti [a,b], Anna Maria Bianchi [b], Marta Parazzini [c], Natale Maiorana [a], Marta Bonato [c], Rosanna Ferrara [a], Giorgia Libelli [d], Kora Montemagno [a], Roberta Ferrucci [a,e], Alberto Priori [a,e], Tommaso Bocci [a,e,*]

[a] "Aldo Ravelli" Center for Neurotechnology and Experimental Brain Therapeutics, Department of Health Sciences, University of Milan, Via Antonio di Rudinì 8, 20142 Milan, Italy
[b] Department of Electronics, Information and Bioengineering, Politecnico di Milano, Piazza Leonardo da Vinci, 32, 20133 Milan, Italy
[c] Institute of Electronics, Computer and Telecommunication Engineering (IEIIT), CNR, 20133 Milan, Italy
[d] Neurology Unit, Department of Medicine and Surgery, University of Parma, Via Gramsci 14, 43126 Parma, Italy
[e] Clinical Neurology Unit, "Azienda Socio-Sanitaria Territoriale Santi Paolo E Carlo", Department of Health Sciences, University of Milan, Via Antonio di Rudinì 8, 20142 Milan, Italy

HIGHLIGHTS

- Multi-electrode tDCS might help steering the electric field, also at deep level.
- Bilateral motor tDCS with extracephalic reference might induce significant electric fields at deep brain level.
- Bilateral motor anodal tDCS with cathode over right hemisphere might selectively affect brainstem reflexes.

ARTICLE INFO

Article history:
Accepted 12 August 2023
Available online 29 August 2023

Keywords:
Neuromodulation
tDCS
Computational Model
Blink Reflex
Masseter Inhibitory Reflex

ABSTRACT

Objective: To assess whether monopolar multi-electrode transcranial direct current stimulation (tDCS) montages might selectively affect deep brain structures through computational predictions and neurophysiological assessment.
Methods: Electric field distribution in deep brain structures (i.e., thalamus and midbrain) were estimated through computational models simulating tDCS with two monopolar and two monopolar multi-electrode montages. Monopolar multi-electrode tDCS was then applied to healthy subject, and effects on pontine and medullary circuitries was evaluated studying changes in blink reflex (BR) and masseter inhibitory reflex (MIR).
Results: Computational results suggest that tDCS with monopolar multi-electrode montages might induce electric field intensities in deep brain structure comparable to those in grey matter, while neurophysiological results disclosed that BR and MIR were selectively modulated by tDCS only when cathode was placed over the right deltoid.
Conclusions: Multi-electrode tDCS (anodes over motor cortices, cathode over right deltoid) could induce significant electric fields in the thalamus and midbrain, and selectively affect brainstem neural circuits.
Significance: Multi-electrode tDCS (anodes over motor cortices, cathode over right deltoid) might be further explored to affect brainstem activity, also in the context of non-invasive deep brain stimulation.

1. Introduction

Transcranial direct current stimulation (tDCS) is a non-invasive brain stimulation (NIBS) technique which has gained great interest in recent years, due to its safety (Antal et al., 2017), feasibility (Siebner et al., 2004; Woods et al., 2016), affordability (Manto et al., 2021), and available clinical evidences (Lefaucheur et al., 2017). Low-amplitude (typically 1–2 mA) direct current is injected in the brain via scalp electrodes, and generates small electrical fields (EF) responsible of biological (Guidetti et al., 2022b) and, ultimately, behavioural changes (D'Urso et al., 2015; Peterchev et al., 2012), together with the individual anatomy (Opitz et al., 2015).

* Corresponding author at: Center for Neurotechnology and Experimental Brain Therapeutics, Department of Health Sciences, University of Milan, Via Antonio di Rudinì 8, 20142 Milan, Italy.
E-mail address: tommaso.bocci@unimi.it (T. Bocci).

https://doi.org/10.1016/j.clinph.2023.08.011
1388-2457/

Computational models (Gomez-Tames et al., 2020; Parazzini et al., 2012, 2011; Rashed et al., 2020; Thomas et al., 2019) and in vivo recordings (Guidetti et al., 2022a) reported that tDCS can generate significant EF in subcortical regions, possibly modifying their activity. However, stimulation in depth is not focal (Huang and Parra, 2019) and tDCS-induced EF is hardly controllable (Datta et al., 2009). Physically, the distribution of the EF depends upon the temporal (e.g., waveform) and spatial (e.g., electrodes' position) characteristics of the current injected (Peterchev et al., 2012). Therefore, several authors have tried to steer the EF by setting number and position of scalp electrodes – a strategy called multi-electrode tDCS (Dmochowski et al., 2011; Guler et al., 2016; Ruffini et al., 2014; Sadleir et al., 2012; Wagner et al., 2016). Evidence suggests that this approach might be able to direct the current toward or away from specific brain areas (Sadleir et al., 2012) and to induce more focalized (Park et al., 2011; Ruffini et al., 2014; Wagner et al., 2016) and intense (Khorrampanah et al., 2020; Wagner et al., 2016) stimulation at brain cortical targets (Khan et al., 2022; Park et al., 2011). Sadleir et al. (2012) successfully demonstrated that optimized multi-electrode montages could not only steer current in deep brain structures (namely, nuclei accumbens), but also avoid the left inferior frontal gyrus while targeting basal ganglia, and vice versa (Sadleir et al., 2012). Huang et al. (2019) (Huang and Parra, 2019) computationally demonstrated that tDCS applied with an appropriate multi-electrode montages can induce significant stimulation in deep targets, with cerebrospinal fluid directing currents deep into the brain. Taken together, these findings have fostered the interest in tDCS as a non-invasive deep brain stimulation (NDBS) technique (Huang and Parra, 2019), a new field of research that aims to affect deep brain regions' activity through NIBS methods (Bikson and Dmochowski, 2020) without resorting to neurosurgery as in other neurostimulation techniques (Priori et al., 2021).

Here, we investigate the ability of a series of tDCS montages to steer the EF in deep brain structures by applying the multi-electrode approach. We arbitrarily considered extracephalic montages, i.e., placing two anodes over the scalp and one cathode far from the scalp (namely, over the right deltoid and over the 10th thoracic vertebra). Indeed, several studies suggest that the extracephalic reference induces a concentration of currents (Mendonca et al., 2011; Noetscher et al., 2014) and greater EF in deeper brain structures (e.g., cerebellum, thalamus and striatum midbrain, pons and medulla) compared to cephalic montages (Bai et al., 2014; Parazzini et al., 2013). We aimed to:

1. Estimate the EF in 4 regions of interest (ROIs - grey matter, hippocampus, thalamus and mid-brain) as modelled in an MRI-based realistic human head model (Christ et al., 2010).
2. Validate the predictions for those stimulation montages which had higher values of EF in deep brain structures by analysing electrophysiological responses (blink reflex – BR, and masseter inhibitory reflex - MIR) reflecting the activity of pontine and low medullary neuronal circuitries. The neurophysiological study is thought to extend our computational data, as it refers to anatomical structures deeper than those analysed by MRI-based human models.

2. Materials e methods

2.1. High-Resolution computational model

In the computational study, the quasi-static Laplace equation was solved by the simulation platform Sim4life (from ZMT Zurich Med Tech AG, Zurich, Switzerland, https://www.zurichmedtech.com) to determine the tDCS-induced electric potential (ϕ) distribution in human head tissue:

$$\nabla\cdot(\sigma\nabla\phi) = 0$$

where σ is the electrical conductivity of the human tissues. The distribution of EF was obtained by means of the equations:

$$EF = -\nabla\phi$$

A finite element method (FEM) realistic human model based on high-resolution magnetic resonance images of healthy volunteers (Christ et al., 2010) was used. The human model "Ella" (a 26-year-old female adult) consisted of 76 different tissues with dielectric properties assigned according to literature data (Gabriel et al., 2009, 1996).

We modelled the electrodes in the following positions, according to the 10–20 system, as previously explored (Cogiamanian et al., 2007; Fertonani et al., 2010; Mesquita et al., 2020; Parazzini et al., 2013) (see Fig. 1):

- I) Montage A1: active electrode over the vertex, return electrode over right deltoid.
- II) Montage A2: active electrode over C3 and C4, return electrode over right deltoid.
- III) Montage B1: active electrode over the vertex, return electrode over the spinal process of the 10th thoracic vertebra.
- IV) Montage B2: active electrode over C3 and C4, return electrode over the spinal process of the tenth thoracic vertebra.

For comparative purposes, we considered a fifth cephalic montage (Montage C), i.e., active electrode over left M1 (C3) and return electrode over the right supraorbital region (Fp2). Electrodes were modelled as a rectangular pad conductor (5x5 cm, $\sigma = 5.9 \times 10^7$ S/m) with a thickness of 1 mm. Their lower surface is separated from the skin by a layer of 5 mm of conductive gel ($\sigma = 1.4$ S/m), shaped as the conductor itself. In each computational simulation, the upper surface of each electrode was set to a uniform electrical potential and the potential difference between the electrodes was adjusted so that the current injected through the anode(s) was the desired value (2 mA).

For each simulation, the model (i.e., human model plus electrodes) was placed in a surrounding bounding box filled with air and the model was trunked at the pelvis level for electrode montages A1-B2 and at the shoulder level for the electrode montage C. The boundaries of the bounding box were treated as insulated except the truncation section of the Ella model, which was assigned with a boundary condition of continuity of the current. Continuity of the tangential component of EF was applied at each tissue-to-tissue boundary. At the interface between the skin and the air, the current density was set to be parallel to the surface. The computational domain was discretized by uniform rectilinear grid, with a mesh step equal to 1 mm to allow a good discretization of the anatomical model.

For each montage model, the amplitude of EF was computed and analysed in 4 different ROIs: grey matter (GM), hippocampus (HPC), mid-brain (MB), and thalamus (THA) (see Fig. 2, first row). For each EF distribution, we estimated the "peak" (i.e., the 99th percentile), the median amplitude, the 25th and 75th percentile. Furthermore, we estimated the percentage of area of hippocampus, mid-brain, and thalamus where the amplitude of EF was greater than 25% (V25), 30% (V30), and 50% (V50) of 99th percentile in grey matter. All these values have been calculated as normalized to the 99th percentile of E in the grey matter for each montage.

2.2. Neurophysiological study

2.2.1. Subjects

The experimental study was conducted on ten healthy volunteers (mean ± SD age: 31.5 ± 9.7, 5 women). The exclusion criteria were as follows: 1) age < 18 years; 2) history and/or current signs

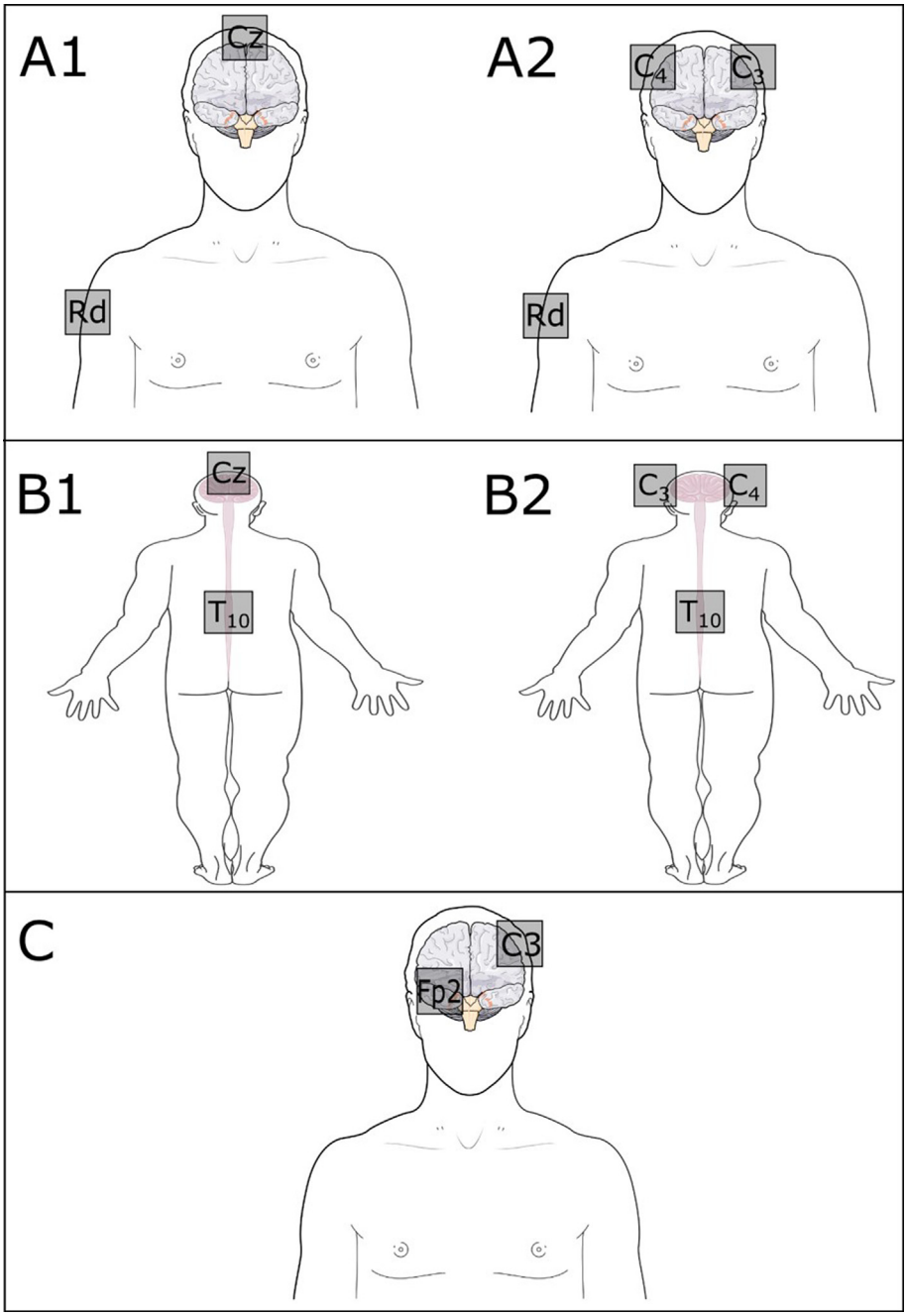

Fig. 1. Transcranial direct current stimulation (tDCS) montages for computational models. A1) Active electrode: Cz, return electrode: right deltoid; **A2)** Active electrodes: C3, C4, return electrode: right deltoid; **B1)** Active electrode: Cz, return electrode: T10; **B2)** Active electrodes: C3, C4, return electrode: T10; **C)** Active electrode: C3, Return electrode: Fp2. Positions of electrodes were considered according to 10–20 system.

or symptoms of major neurologic, neuropsychological, and psychiatric diseases, as excluded by clinical history and anamnestic interview; 3) pregnancy; 4) presence of a pacemaker, intracranial metal, or spinal cord stimulators; 5) history and/or current signs or symptoms of dental pathologies and/or surgery involving the alveolar branch of the mental nerve. The study protocol followed the Declaration of Helsinki and was approved by the Ethics Committee of the ASST Santi Paolo e Carlo - Hospital of Milan. All subjects gave written informed consents before the participation.

2.2.2. Study protocol

In this experimental, assessor-blinded, randomized crossover study, each volunteer underwent bilateral motor cortex anodal tDCS (2 mA for 20 min) with cathode over right deltoid (condition E1) and over T10 (condition E2) in two different sessions separated by a washout period of at least 1 week to avoid possible carryover effect. We chose to apply these experimental stimulation protocols since they resulted in the highest values of EF in ROIs in computational simulations, among the montages considered. A further control condition was considered (condition Ec – 1.75 mA for 20 min), where anode was placed over left motor cortex, and cathode over contralateral supraorbital region (see Supplementary Figure S1). The order of the experimental conditions was randomized across the subjects (see Supplementary Figure S2). BR and MIR were recorded immediately before (T0) and after (T1) the stimulations.

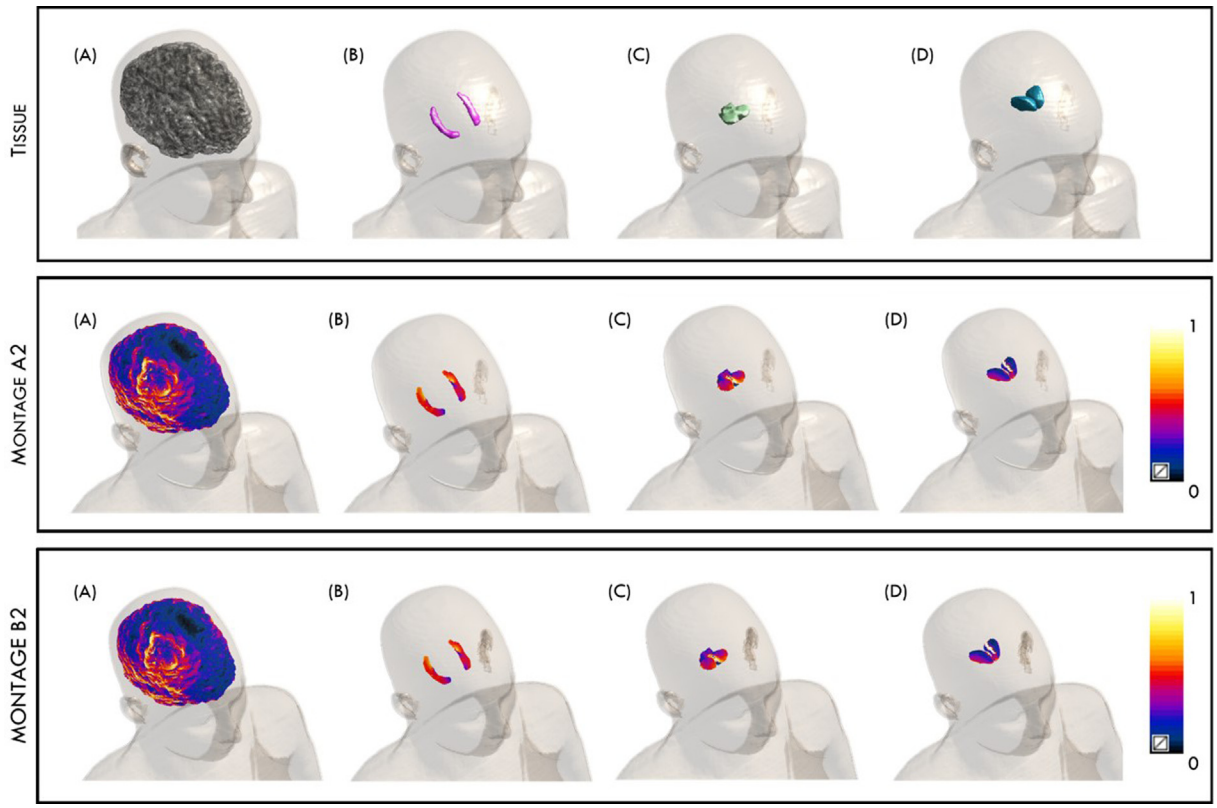

Fig. 2. First row: the 4 different brain structures considered as region of interest (ROIs) - grey matter (A), hippocampus (B), mid-brain (C), and thalamus (D). **Second row:** the view of the estimated electric field amplitude distribution over grey matter (A), hippocampus (B), midbrain (C), and thalamus (D) for montage A2 (active electrodes over C3, C4; return electrode over right deltoid). **Third row:** view of the estimated EF amplitude distribution over grey matter (A), hippocampus (B), mid-brain (C), and thalamus (D) for montage B2 (active electrodes over C3, C4; return electrode over the spinal process of the tenth thoracic vertebra). The values are normalized with respect to the 99th percentile in grey matter.

2.2.3. tDCS experimental protocol

DC stimulation was applied by a stimulator (HDCStim, Newronika, Italy) connected to silicone rubber pad electrodes with thickness of 1 mm and an area of 35 cm^2 (7 × 5 cm^2) for the anodes, 48 cm^2 (8 × 6 cm^2) for the cathode. Conductive gel was applied between the electrodes and the skin to reduce and stabilize contact impedance during stimulation. We clinically replicated the multi-electrode montages that predicted the highest intensities of EF in MB and THA, as shown in the previous computational study. We chose Montage A2 and Montage B2 because the EF amplitudes in deep regions were comparable to those in grey matter, with higher values compared to the other montages tested. Therefore, anodes were applied bilaterally over the motor cortex (C3 and C4 scalp positions of the International EEG 10/20 system), while cathodes were placed over left deltoid (condition E1) or over T10 (condition E2). As control condition, a third montage (anode over C3, cathode over Fp2) was considered (condition Ec). DC was applied at 2 mA for E1, E2 conditions, and 1.75 mA for Ec condition, to keep the current density (current strength divided by electrode size) constant in all the conditions (current density = 0.028 mA/cm^2) for 20 min, with the first 30 s as ramp-up and the last 30 s as ramp down. We considered values of current density way lower than limits commonly accepted (Bikson et al., 2009).

2.2.4. Blink reflex recording

Two of the investigators, who were blinded to the stimulation setting, performed the evaluation, and took the measurements. During the assessments, participants were sitting in a comfortable chair and instructed to keep their eyes open and fix a target placed 1 m in front of them. The right and left supraorbital nerve were consecutively stimulated through a pair of silver chloride cup electrodes (cathode over the supraorbital foramen; anode 2 cm above). A constant current with pulse width 200 μs and inter-trial interval ranging between 25 and 35 s to avoid habituation was used as stimulation (Aramideh and Ongerboer De Visser, 2002; Esteban, 1999). The stimulation point, at both sides, was marked with a pencil in order to ensure reproducibility between different assessment sessions (T0 and T1). EMG activity was bilaterally recorded from the orbicularis oculi muscle, via surface electrodes (active electrode over the mid-lower eyelid; reference electrode laterally to the lateral canthus). A total of 8 responses was recorded on each side. Electromyographic signal (band-pass 10 Hz–10 kHz, sampling rate 20 kHz, sensitivity set 500 μV/Div; sweep speed 10 ms/Div) was collected from superimposed traces and stored for offline analysis. Recording electrodes were kept in the same position on the skin during tDCS. The reflex threshold (i.e., the lowest stimulus intensity resulting in a RI reproducible in the subject - mV), as well as latencies (ms) of the two main components, formally named RI and RII (ipsilateral and contralateral), was considered for statistical analysis (see Supplementary Figure S3). These two responses originate from different pathways, at a low-pontine and medullary level respectively (Bocci et al., 2021; Esteban, 1999).

2.2.5. Masseter inhibitory reflex recording

Two of the investigators, who were blinded to the stimulation setting, performed the evaluation, and took the measurements. The method of recording the masseter inhibitory reflex is reported in details elsewhere (Schoenen, 1993). Briefly, subjects were asked to clench their teeth as strong as possible, as confirmed by audio-visual examination of electromyographic activity. Sweep speed

was set at 50 ms per division and band-pass filters at 20 HZ to 10 kHZ. EMG signals were recorded through surface electrodes from the masseter muscles bilaterally, with the active electrode placed over the lower third of the muscle belly and the reference approximately 2 cm below the mandibular angle (Cruccu and Deuschl, 2000; Kennelly, 2019). Recording electrodes were kept in the same position on the skin during tDCS. Then, the inferior alveolar branch of the mental nerve was stimulated transcutaneously with the cathode positioned over the mental foramen and the anode placed 1 cm laterally. An electrical square-wave pulse (0.1 ms duration) was delivered, and the stimulus intensity set at 2.5 times the reflex threshold (range 15–45 mA, approximately 8–10 times the sensory threshold). The stimulation point was marked with a pencil to ensure reproducibility between different assessment sessions (T0 and T1). The lingual nerve was not stimulated, as this alternative procedure for MIR recording is usually devoted to the assessment of iatrogenic damage after third molar extraction. Eight traces were recorded for each side and signals superimposed for off-line analyses. Both onset latencies and duration of the two Silent Periods (formally named SP1 and SP2) was considered for statistical analysis (see Supplementary Figure S4). These periods are mediated by non-nociceptive A-beta afferents through oligosynaptic (SP1) and polysynaptic (SP2) circuits, partly overlapping with those involved in BR generation, with a slightly more dorsal and lateral localization regarding SP2 as compared to RII (Cruccu et al., 2005, 1989).

2.2.6. Statistical analysis

Normal distributions of the dependent variables were assessed via Shapiro-Wilk Test for normality, which is the more appropriate method for small sample sizes (Mishra et al., 2019). All data sets passed the test ($p > 0.05$), therefore parametric analysis was considered. tDCS-induced changes in neurophysiological outcomes at each time point were assessed via two-way Repeated Measures ANOVA (RM-ANOVA), with treatment protocol as "between factor" to analyse the effect of Time and Treatment on neurophysiological outcomes. Sphericity assumptions was verified through Mauchly's test of sphericity, and Greenhouse-Geisser correction was applied when needed. Multiple comparisons were performed through Holm-Bonferroni Post Hoc test.. In all the analysis, a p-value < 0.05 was set as significant. The data were analysed using JASP v. 0.16.3 for Windows (JASP Team, 2022).

3. Results

3.1. Electric field estimations

Fig. 3 shows the amplitude of EF in the HPC, MB, and THA for the five electrode montages, as normalized to the 99th percentile of EF in the grey matter for each montage. For each montage, medians, 25th and 75th percentiles in deeper regions are roughly comparable to those in the grey matter when the return electrode is extracephalic, with peak values always above 65% of the peak in the grey matter (Fig. 3 - A1, A2, B1 and B2). However, montage A2 and B2 (i.e., multi-electrode montages with 2 active electrodes over the skull) resulted in higher normalized 25th percentiles, medians, and 75th percentiles in deeper brain structures. Conversely, values of EF in montage C are remarkably lower compared to the other montages considered for all the ROIs, with peaks always lower than 33% of the peak in the grey matter (Fig. 3 – C). Fig. 2 (second and third row) shows the graphical views of the amplitude distribution of EF in GM, HPC, MB, and THA for Montage A2 and B2. We chose to show only these montages' graphical outcomes because they predicted the highest intensities of EF in deep structures and were chosen for clinical applications. As for the volume percentage, Fig. 4 shows the V25s, V30s and V50s of HPC, MB, and THA for the five electrode montages, as normalized to the 99th percentile of EF in the grey matter for each montage. Montages with return electrode over the shoulder (Montage A1, Montage A2) and the spine (Montage B1, Montage B2) had values one order of magnitude greater than those in Montage C, with values of V50 one hundred times higher. Montages A1 and B1 showed a similar pattern of percentages, with close V25, V30 and V50 (Fig. 4). Montage A2 and B2 resulted in similar volumes for each structure as well, but with remarkably higher values both for V25, V30 and V50 compared to A1 and B1 montages (Fig. 4).

3.2. Neurophysiological outcomes

RM ANOVA disclosed no significant Time or Time*Treatment effects for right BR threshold, RII ipsilateral and RII contralateral latency; left BR threshold, RII ipsilateral and RII contralateral latency; MIR threshold, SP1 latency, SP2 latency and duration ((for all the analysis, $p > 0.05$ – see Table 1). However, a statistically significant effect of Time was found for RII latency of right BR [$F(1) = 10.754$, $p = 0.003$] and left BR [$F(1) = 7.466$, $p = 0.01$], and for SP1 duration of MIR [$F(1) = 7.589$, $p = 0.01$]. In details, RI latency of right BR significantly increased ($p = 0.003$), as RI latency of left BR ($p = 0.01$), while SP1 duration of MIR significantly decreased ($p = 0.01$). A significant interaction Time*Treatment was found for RI latency of right BR ($F(2, 1) = 4.498$, $p = 0.021$), with post-hoc analysis revealing a significant decrease between T0 and T1 with stimulation E1 ($p = 0.004$, Holm-Bonferroni Post Hoc test.) (see Fig. 5).

4. Discussion and conclusions

In this study, we assessed the trends of EF distributions in 4 ROIs (GM, HPC, MB and THA) during bi- and multielectrode tDCS with reference over the right deltoid and over the spinal process of the 10th thoracic vertebra, and compared them with a control cephalic montage- tDCS. Our results suggest that extracephalic montages might induce a deeper and more focal distribution of EF. Then, we clinically tested these predictions applying the montages which resulted in higher EF values (i.e., bilateral motor cortex anodal tDCS with cathode over right deltoid and over T10) to healthy subjects. Clinical findings seem to confirm that bilateral motor cortex anodal tDCS with extracephalic cathode (over right deltoid, but not over T10) induces changes in BR, whereas control cephalic montage leaves these parameters unchanged.

Several computational studies have suggested that setting number and position of scalp electrodes during tDCS could help in increasing the intensity and focality of stimulation in a target zone (D'Urso et al., 2022; Khorrampanah et al., 2020; Wagner et al., 2016). For example, Khorrampanah et al., 2020 (Khorrampanah et al., 2020) demonstrated that arbitrarily chosen multi-electrode montages could be optimized to induce a maximum EF distribution in targeted region which was higher compared to High-definition tDCS (HD-tDCS), also at the inner layers of the head. It is worth pointing out that HD-tDCS is a technically enhanced version of tDCS, which is believed to be more focal (Kuo et al., 2013). Also, some authors proposed that the same results might be optimized for deep brain targets (Huang et al., 2019; Sadleir et al., 2012). However, none of these studies were clinically confirmed, nor considered to use an extracephalic electrode (namely, the cathode - classically, placed over right deltoid or the spine (Bikson et al., 2019)). Indeed, the position of the return electrode, for a fixed position of active electrode, affects the tDCS-induced current distribution and brain modulation (Mendonca et al., 2011; Nitsche and Paulus, 2000). Although little is known about the actual current passing through the brainstem and other

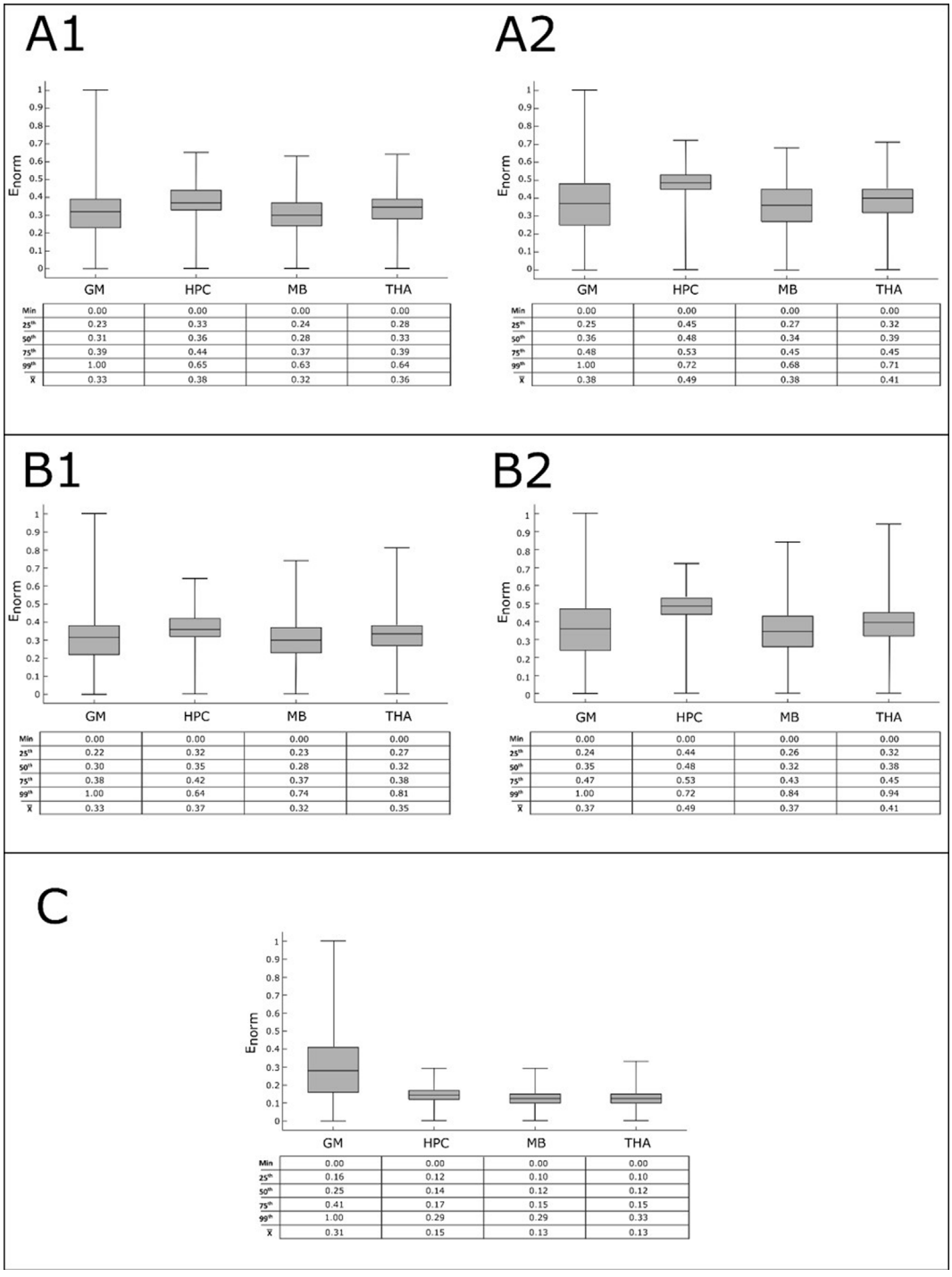

Fig. 3. Quantitative distributions of E in the grey matter (GM), hippocampus (HPC), mid-brain (MB), and thalamus (THA) for montages (A1, B2, B1, B2, C) in the computational models. The values (minimum, 25th percentile, median, 75th percentile, 99th percentile, mean) are displayed with respect to the 99th percentile in grey matter.

subcortical nuclei when an extracephalic cathode is used (Im et al., 2012; Parazzini et al., 2014, 2013), several studies have investigated such issue (Bai et al., 2014; Im et al., 2012; Mendonca et al., 2011; Noetscher et al., 2014; Parazzini et al., 2013). It has been computationally suggested that moving the cathode outside the scalp induces a concentration of currents (Mendonca et al., 2011; Noetscher et al., 2014). When compared to cephalic configurations, extracephalic montages induced significant amount of current under the active electrode, rather than between the electrodes (Mendonca et al., 2011; Noetscher et al., 2014). Although these results are still matter of debate (Im et al., 2012), we observed that in Ec condition (i.e., cephalic configuration), V25 and V30 were more than 10 times, and V50 more than 100 times, lower compared to other extracephalic montages (A1, A2, B1 and B2). This observation suggests that extracephalic configurations could induce a focalisation of electric distribution. Also, our results showed that trends of EF in THA and MB were comparable to those in the GM for extracephalic montages, suggesting that they might

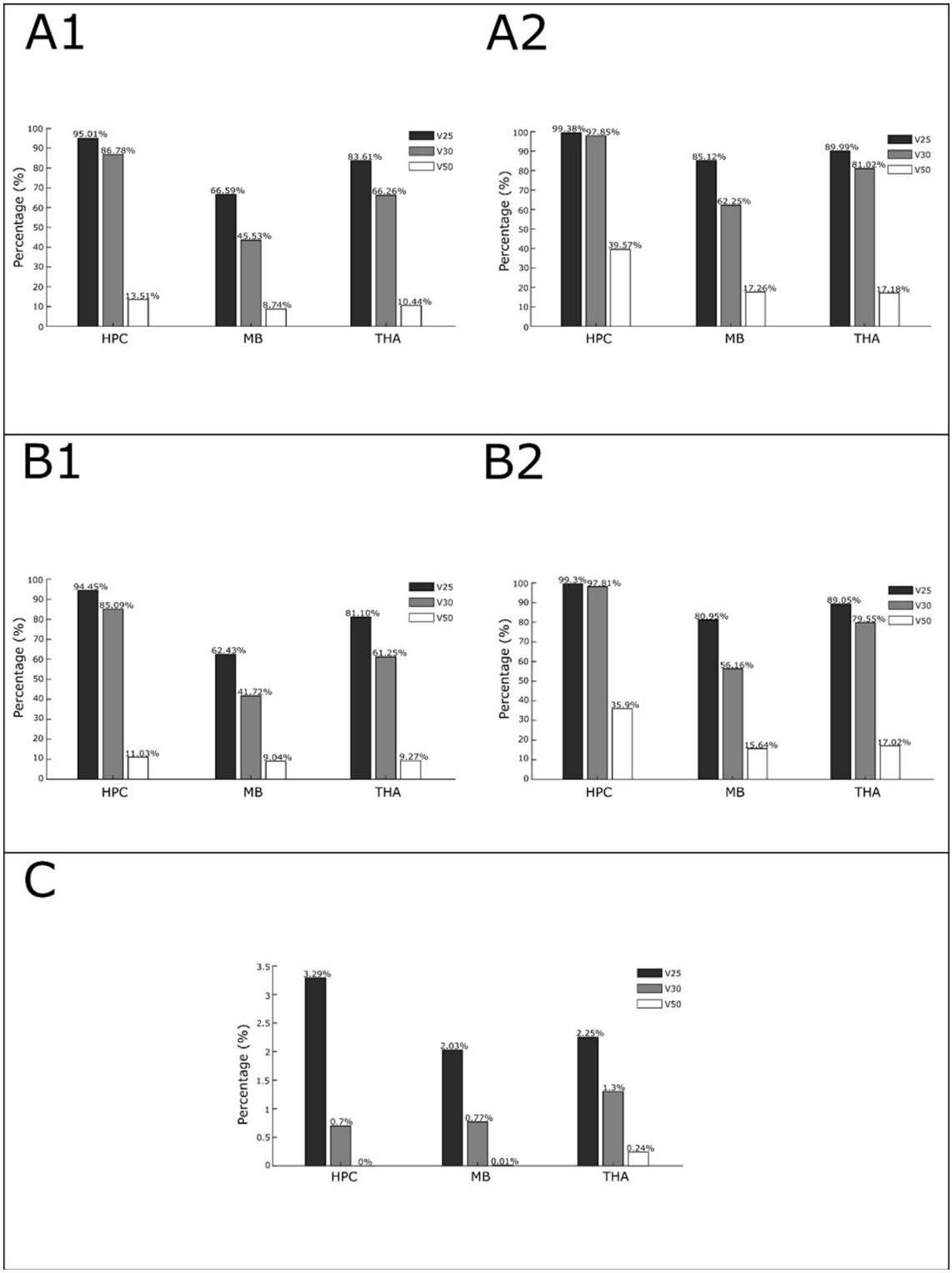

Fig. 4. Bar chart representing the distribution of the electric field amplitude as V25 (percentage of volume greater than 25% of 99th percentile in grey matter), V30 (percentage of volume greater than 30% of 99th percentile in grey matter), and V50 (percentage of volume greater than 50% of 99th percentile in grey matter) in hippocampus (HPC), midbrain (MB) and thalamus (THA) for montages (A1, B2, B1, B2, C). The values are displayed with respect to the 99th percentile in grey matter.

result in substantially greater depth of stimulation compared to C3-Fp2 configuration. Although the assumption is still controversial (Im et al., 2012), several models in literature confirm our predictions (Bai et al., 2014; Noetscher et al., 2014; Parazzini et al., 2013). For example, for fixed anode placement (over left frontal cortex), cathode over the right deltoid developed an EF in the cerebellum, deep central structures (THA, striatum) and brainstem, greater than those developed with cathode over contralateral supraorbital region (Bai et al., 2014). Since neurons in deep brain regions are directly sensitive to weak electric fields (Francis et al., 2003; Reato et al., 2010) and to DC stimulation (Bikson et al., 2004; Chakraborty et al., 2018; Kronberg et al., 2020), an

Table 1
Neurophysiological assessments. Characteristics of blink reflex (threshold, RI latency, RII latency ipsilateral, RII latency contralateral) and masseter inhibitory reflex (threshold, latency SP1, duration SP1, latency SP2, duration SP2) are reported at T0 and T1, according to the treatment condition (A, B, or C) group (anodal or sham tsDCS). Values are expressed mean values ± standard error (S.E.), pValue refers to two ways Repeated Measures ANOVA.

	Condition E1		**Condition E2**		**Condition Ec**			**Two ways RM ANOVA**
	T0	T1	T0	T1	T0	T1	Time (pValue)	Time*Treatment (pValue)
Blink Reflex (R)								
Threshold	17.47 ± 2.19	18.52 ± 2	17.33 ± 2.19	17.15 ± 2.05	17.53 ± 1.64	20.06 ± 2.79	0.61	0.53
RI latency	10.6 ± 0.22	9.89 ± 0.23	10.21 ± 0.21	9.87 ± 0.13	10.58 ± 0.35	10.63 ± 0.31	**0.003**	**0.021**
RII latency ipsilateral	30.53 ± 1.28	31.57 ± 1.39	30.54 ± 1.26	29.60 ± 0.80	30.75 ± 0.92	31.01 ± 0.94	0.75	0.09
RII latency contralateral	31.01 ± 1.36	32.05 ± 1.51	31.09 ± 1.15	31.07 ± 0.81	31.88 ± 1.44	32.31 ± 1.45	0.17	0.43
Blink Reflex (L)								
Threshold	17.56 ± 2.11	18.41 ± 1.8	17.22 ± 1.94	18.06 ± 1.84	16.62 ± 1.28	20.50 ± 3.10	0.58	0.65
RI latency	10.57 ± 0.27	10.08 ± 0.22	10.23 ± 0.22	9.80 ± 0.23	10.52 ± 0.33	10.43 ± 0.21	**0.01**	0.39
RII latency ipsilateral	30.1 ± 1.41	30.3 ± 1.08	30.45 ± 1.33	28.36 ± 0.72	30.73 ± 1.05	31.43 ± 1.02	0.49	0.11
RII latency contralateral	31.29 ± 1.70	32.24 ± 1.18	31.73 ± 1.10	29.98 ± 0.70	31.17 ± 1.44	32.20 ± 1.41	0.90	0.10
Masseter Inhibitory Reflex								
Threshold	18.3 ± 1.38	18.34 ± 1.35	18.48 ± 0.92	17.78 ± 1.23	16.83 ± 1.40	16.20 ± 1.73	0.51	0.87
Latency SP1	14.33 ± 0.65	14.06 ± 0.50	13.65 ± 0.79	12.93 ± 0.62	14.55 ± 0.55	14.47 ± 0.57	0.18	0.58
Duration SP1	13.12 ± 1.03	17.06 ± 2.31	13.66 ± 1.45	16.55 ± 1.80	13.27 ± 1.20	14.21 ± 1.28	**0.01**	0.44
Latency SP2	49.99 ± 2.51	49.06 ± 2.43	50.67 ± 3.4	49.63 ± 2.54	50.26 ± 1.53	50.41 ± 1.24	0.64	0.92
Duration SP2	29.84 ± 3.14	29.31 ± 2.97	31.39 ± 5.57	28.8 ± 4.15	31.22 ± 2.91	30.30 ± 2.90	0.40	0.80

R = right; L = left; SP1 = silent period; Condition E1 = anodes over C3 and C4, cathode over right deltoid; Condition E2 = anodes over C3 and C4, cathode over the 10th thoracic vertebra; Condition Ec = anode over C3, cathode over Fp2. Positions of electrodes were considered according to 10–20 system.

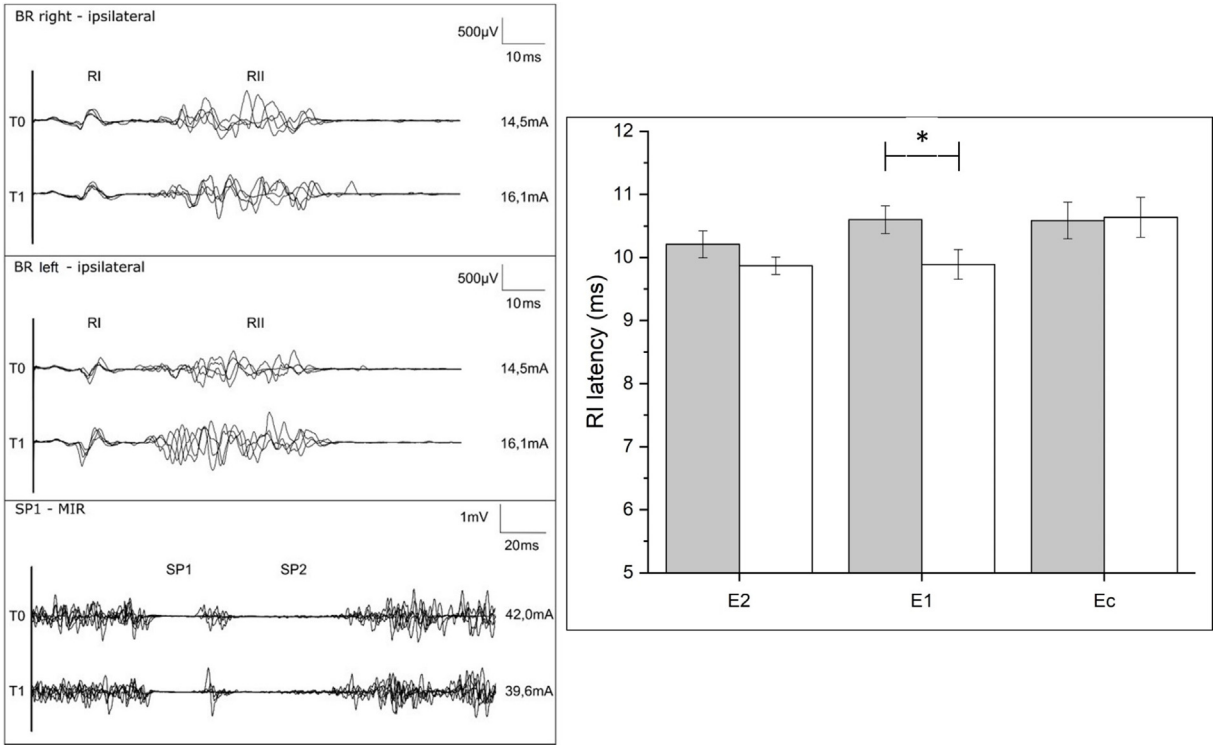

Fig. 5. Neurophysiological changes in condition E1 (anodes over C3 and C4, cathode over right deltoid). Left. Exemplificative averaged traces of blink reflex (right), blink reflex (left)(patient's age = 55), and masseter inhibitory reflex (patient's age = 25) recorded before (T0) and after (T1). Side values refer to stimulation intensities. **Right**. Changes in RI latency of right BR (*p < 0.05, Holm-Bonferroni Post Hoc test.).

effect similar to those induced by tDCS at cortical level might be expected.

Our neurophysiological findings might confirm computational predictions, but only for E1 condition. Bimotor anodal tDCS with cathode over right deltoid reduced latency of RI in right BR, suggesting a neuromodulatory effect on brainstem. Both BR and MIR arcs relies on brainstem neural circuits, which integrate afferent limb (respectively, ophthalmic division of the trigeminal nerve and mental branch of the trigeminal nerve) with efferent limb (respectively, facial nerve and mandibular branch of the trigeminal nerve) (Aramideh and Ongerboer De Visser, 2002; Cosentino et al., 2022; Cruccu et al., 1990; Kugelberg, 1952). In details, for BR, afferent stimuli elicit two responses, RI and RII. For RI response, the sensory stimulus is conducted through the pons, relayed in the vicinity of the main sensory nucleus of the trigeminal nerve (Kimura, 1975; Shahani and Young, 1972), and, finally, reaches the ipsilateral facial nucleus in the lower pontine tegmentum (Esteban, 1999). For ipsilateral RII, the afferent impulse is conducted through the descending spinal tract of the trigeminal nerve in the pons and medulla oblongata, relayed in the caudal spinal

trigeminal nucleus by a medullary pathway (Kimura and Lyon, 1972; Ongerboer De Visser and Kuypers, 1978), and ascends bilaterally to reach the facial nuclei in the pons thus inducing contralateral RII responses (Holstege et al., 1986; Ongerboer De Visser and Kuypers, 1978). For MIR, after stimulation, the impulse reaches the pons through the sensory mandibular root of the trigeminal nerve (Ongerboer De Visser and Goor, 1976). In the ipsilateral trigeminal motor nucleus, an inhibitory interneuron projects onto jaw-closing motoneurons bilaterally, inducing SP1 response (De Visser et al., 1990). As for SP2 response, stimulus is conducted to the lateral reticular formation, where an inhibitory interneuron conducts it to ipsilateral and contralateral trigeminal motoneurons (De Visser et al., 1990). In order to integrate computational data with the neurophysiological outcome, we can hypothesize that tDCS may interfere with diencephalic nuclei strictly connected to pontine and medullary areas from which BR originates; in particular, a cholinergic downstream has been recently identified between the hypothalamic paraventricular nucleus and different brainstem nuclei (comprising reticular formation, locus ceruleus, dorsal raphe nucleus and motor nucleus of the vagus) (Fearon et al., 2021). However, BR parameters might be influenced by structures above the brainstem, e.g., motor cortex and basal ganglia (Esteban, 1999). Computational studies report, also for multi-electrode tDCS, that it is not possible to avoid delivering current to peripheral cortical regions while targeting deep structures (Sadleir et al., 2012; Wagner et al., 2016). In 2016, Cabib et al. (Cabib et al., 2016) found that biemispheric (anode-C3, cathode-C4) and uniemispheric (anode-C3, cathode-Fp3) tDCS significantly changed BR excitability, and explained this result with a tDCS-induced supranuclear activation conveyed via cortico-reticular (Nonnekes et al., 2014) or cortico-nuclear connections (Berardelli et al., 1983; Fisher et al., 1979; Kuypers, 1958). Also, both BR and MIR arc rely on trigeminal nerve, which is constantly activated during tDCS as suggested by the fact that almost all subjects report different types of sensations under the electrodes (i.e., in the sensory territory of trigeminal nerve) (Nitsche et al., 2008). The continuous sensory inputs via trigeminal afferents on brainstem interneurons may sensitize reflex circuits (Bologna et al., 2010; Manca et al., 2001; Mao and Evinger, 2001) and lead to the enhancement of reflex excitability (Cabib et al., 2016).

In our study, we performed a control stimulation condition (Ec) to exclude that activation of descending cortical pathways and/or sensitization of trigeminal nerve could confound the results. Indeed, control montage had electrodes on both left and right trigeminal territory of innervation, and the anode was placed over left motor cortex. Although this montage was slightly different than previous study (Cabib et al., 2016), still significant changes in BR were found only for E1 stimulation. This might suggest a frank effect of stimulation. Furthermore, we found changes only in RI latency, which is reported to be resistant to suprasegmental, supratentorial, and cognitive influences (Cruccu and Deuschl, 2000). We found no evidence of changes in RII, which is reported to be strongly susceptible to suprasegmental, cortical and cognitive influences (Kimura et al., 1994). Cortical influences for RII generation are confirmed by data showing that NIBS applied over the primary motor cortex are able to modulate RII recovery cycle only, without significant after-effects on RI amplitudes and latencies (De Vito et al., 2009). Moreover, in order to avoid cortical influences possibly underlying our results, it should be considered that differences in tDCS montages, as well as electrodes size and number (see supplementary material, Figure S1), impact intracortical excitability in a similar extent, as shown by changes in Short Intracortical Inhibition (SICI), Intracortical Facilitation (ICF) and Short Intracortical facilitation (SICF) using either conventional or high-definition montages (Pellegrini et al., 2021).

The present work has some limitations. As for the computational models, the results were obtained without accounting for interindividual variability which may influence EF magnitude and spatial distribution (Datta et al., 2009), and montages to be tested were arbitrarily chosen and not optimized. Also, the model used only comprised of a limited number of tissues, potentially arising errors from the exclusion of the dielectric properties of other tissues. As for the clinical study, larger population should be tested for confirmations, and investigations targeting neuronal excitability (e.g., TMS studies (Roos et al., 2021),studies assessing trigeminal pathways through paired stimulation (KIMURA, 1973), or considering neurophysiological variables other then the ones we used in this study, including recovery cycle of RII or SP2) should be performed to better elucidate the real effect of stimulation on brainstem circuitry. Finally, as shown for other forms of stimulation (Lamy and Boakye, 2013), both the polarity and depth of tDCS after-effects are likely influenced by genetic polymorphisms (Fritsch et al., 2010; Lamy and Boakye, 2013), as well as by the pre-existing excitability state of either cortical or subcortical structures (Bocci et al., 2014; Lang et al., 2007; Siebner et al., 2004).

In conclusion, our computational and clinical results suggest that multi-electrode tDCS considering two anodes over the motor cortices and the cathode over the right deltoid muscle might induce selective activation of brainstem neuronal circuits. However, given the complexity of brain targeting, future studies might resort to optimization decisional algorithms to achieve an efficient trade-off between intensity, focality, and directionality (Khan et al., 2022). Also, given the importance of inter-subject variability, individualized multi-electrode tDCS should considered (Khan et al., 2022).

Acknowledgments

This research did not receive any specific grant from funding agencies in the public, commercial, or not-for-profit sectors.

Conflict of Interest Statement

M.G., A.M.B., M.P., N.M., M.B., Ros.F., G.L., K.M. and T.B. declare no conflict of interest. R.F. and A.P. are founders and shareholders of Newronika Spa.

We confirm that we have read the Journal's position on issues involved in ethical publication and affirm that this report is consistent with those guidelines.

Data availability statement

Data are available from the corresponding author on request.

Appendix A. Supplementary data

Supplementary data to this article can be found online at https://doi.org/10.1016/j.clinph.2023.08.011.

References

Antal A, Alekseichuk I, Bikson M, Brockmöller J, Brunoni AR, Chen R, et al. Low intensity transcranial electric stimulation: Safety, ethical, legal regulatory and application guidelines. Clin Neurophysiol 2017;128:1774–809. https://doi.org/10.1016/j.clinph.2017.06.001.

Aramideh M, Ongerboer De Visser BW. Brainstem reflexes: Electrodiagnostic techniques, physiology, normative data, and clinical applications. Muscle Nerve 2002;26:14–30. https://doi.org/10.1002/MUS.10120.

Bai S, Dokos S, Ho KA, Loo C. A computational modelling study of transcranial direct current stimulation montages used in depression. Neuroimage 2014;87:332–44. https://doi.org/10.1016/J.NEUROIMAGE.2013.11.015.

Berardelli A, Accornero N, Cruccu G, Fabiano F, Guerrisi V, Manfredi M. The orbicularis oculi response after hemispheral damage. J Neurol Neurosurg Psychiatry 1983;46:837–43. https://doi.org/10.1136/JNNP.46.9.837.
Bikson M, Datta A, Elwassif M. Establishing safety limits for transcranial direct current stimulation. Clin Neurophysiol 2009;120:1033. https://doi.org/10.1016/J.CLINPH.2009.03.018.
Bikson M, Dmochowski J. What it means to go deep with non-invasive brain stimulation. Clin Neurophysiol 2020;131:752–4. https://doi.org/10.1016/j.clinph.2019.12.003.
Bikson M, Esmaeilpour Z, Adair D, Kronberg G, Tyler WJ, Antal A, et al. Transcranial electrical stimulation nomenclature. Brain Stimul 2019;12:1349–66. https://doi.org/10.1016/j.brs.2019.07.010.
Bikson M, Inoue M, Akiyama H, Deans JK, Fox JE, Miyakawa H, et al. Effect of uniform extracellular DC electric fields on excitability in rat hippocampal slices in vitro. J Physiol 2004;557:175–90. https://doi.org/10.1113/jphysiol.2003.055772.
Bocci T, Bulfamante G, Campiglio L, Coppola S, Falleni M, Chiumello D, et al. Brainstem clinical and neurophysiological involvement in COVID-19. J Neurol 2021;268:3598–600. https://doi.org/10.1007/s00415-021-10474-0.
Bocci T, Caleo M, Tognazzi S, Francini N, Briscese L, Maffei L, et al. Evidence for metaplasticity in the human visual cortex. J Neural Transm 2014;121:221–31. https://doi.org/10.1007/s00702-013-1104-z.
Bologna M, Agostino R, Gregori B, Belvisi D, Manfredi M, Berardelli A. Metaplasticity of the human trigeminal blink reflex. Eur J Neurosci 2010;32:1707–14. https://doi.org/10.1111/J.1460-9568.2010.07446.X.
Cabib C, Cipullo F, Morales M, Valls-Solé J. Transcranial Direct Current Stimulation (tDCS) Enhances the Excitability of Trigemino-Facial Reflex Circuits. Brain Stimul 2016;9:218–24. https://doi.org/10.1016/J.BRS.2015.12.003.
Chakraborty D, Truong DQ, Bikson M, Kaphzan H. No Title. Cereb Cortex 2018;28:2786–94.
Christ A, Kainz W, Hahn EG, Honegger K, Zefferer M, Neufeld E, et al. The Virtual Family - Development of surface-based anatomical models of two adults and two children for dosimetric simulations. Phys Med Biol 2010;55:23. https://doi.org/10.1088/0031-9155/55/2/N01.
Cogiamanian F, Marceglia S, Ardolino G, Barbieri S, Priori A. Improved isometric force endurance after transcranial direct current stimulation over the human motor cortical areas. Eur J Neurosci 2007;26:242–9. https://doi.org/10.1111/J.1460-9568.2007.05633.X.
Cosentino G, Maiorano E, Todisco M, Prunetti P, Antoniazzi E, Tammam G, et al. Electrophysiological evidence of subclinical trigeminal dysfunction in patients with COVID-19 and smell impairment: A pilot study. Front Neurol 2022;13:2311. https://doi.org/10.3389/FNEUR.2022.981888/BIBTEX.
Cruccu G, Agostino R, Inghilleri M, Manfredi M, de Visser BWO. The masseter inhibitory reflex is evoked by innocuous stimuli and mediated by A beta afferent fibres. Exp Brain Res 1989 772 1989;77:447–50. https://doi.org/10.1007/BF00275005.
Cruccu G, Deuschl G. The clinical use of brainstem reflexes and hand-muscle reflexes. Clin Neurophysiol 2000;111:371–87. https://doi.org/10.1016/S1388-2457(99)00291-6.
Cruccu G, Iannetti GD, Marx JJ, Thoemke F, Truini A, Fitzek S, et al. Brainstem reflex circuits revisited. Brain 2005;128:386–94.
Cruccu G, Leandri M, Feliciani M, Leandri M. Idiopathic and symptomatic trigeminal pain. J Neurol Neurosurg Psychiatry 1990;53:1034–42. https://doi.org/10.1136/JNNP.53.12.1034.
Datta A, Bansal V, Diaz J, Patel J, Reato D, Bikson M. Gyri-precise head model of transcranial direct current stimulation: Improved spatial focality using a ring electrode versus conventional rectangular pad. Brain Stimul 2009;2:201–7. https://doi.org/10.1016/j.brs.2009.03.005.
De Visser BWO, Cruccu G, Manfredi M, Koelman JHTM. Effects of brainstem lesions on the masseter inhibitory reflex. Functional mechanisms of reflex pathways. Brain. J Neurol 1990;113(Pt 3):781–92. https://doi.org/10.1093/BRAIN/113.3.781.
De Vito A, Gastaldo E, Tugnoli V, Eleopra R, Casula A, Tola MR, et al. Effect of slow rTMS of motor cortex on the excitability of the blink reflex: a study in healthy humans. Clin Neurophysiol 2009;120:174–80. https://doi.org/10.1016/j.clinph.2008.09.024.
Dmochowski JP, Datta A, Bikson M, Su Y, Parra LC. Optimized multi-electrode stimulation increases focality and intensity at target. J Neural Eng 2011;8. https://doi.org/10.1088/1741-2560/8/4/046011 046011.
D'Urso G, Bruzzese D, Ferrucci R, Priori A, Pascotto A, Galderisi S, et al. Transcranial direct current stimulation for hyperactivity and noncompliance in autistic disorder. World J Biol Psychiatry 2015;16:361–6. https://doi.org/10.3109/15622975.2015.1014411.
D'Urso G, Dini M, Bonato M, Gallucci S, Parazzini M, Maiorana N, et al. Simultaneous Bilateral Frontal and Bilateral Cerebellar Transcranial Direct Current Stimulation in Treatment-Resistant Depression-Clinical Effects and Electrical Field Modelling of a Novel Electrodes Montage. Biomedicines 2022;10:1681. https://doi.org/10.3390/biomedicines10071681.
Esteban A. A neurophysiological approach to brainstem reflexes. Blink reflex. Neurophysiol Clin 1999;29:7–38. https://doi.org/10.1016/S0987-7053(99)80039-2.
Fearon C, Lees AJ, McKinley JJ, McCarthy A, Smyth S, Farrell M, et al. On the Emergence of Tremor in Prodromal Parkinson's Disease. J Park Dis 2021;11:261–9. https://doi.org/10.3233/JPD-202322.
Fertonani A, Rosini S, Cotelli M, Rossini PM, Miniussi C. Naming facilitation induced by transcranial direct current stimulation. Behav Brain Res 2010;208:311–8. https://doi.org/10.1016/J.BBR.2009.10.030.
Fisher MA, Shahani BT, Young RR. Assessing segmental excitability after acute rostral lesions: II. The blink reflex. Neurology 1979;29:45–50. https://doi.org/10.1212/WNL.29.1.45.
Francis JT, Gluckman BJ, Schiff SJ. Sensitivity of neurons to weak electric fields. J Neurosci 2003;23:7255–61. https://doi.org/10.1523/jneurosci.23-19-07255.2003.
Fritsch B, Reis J, Martinowich K, Schambra HM, Ji Y, Cohen LG, et al. Direct current stimulation promotes BDNF-dependent synaptic plasticity: potential implications for motor learning. Neuron 2010;66:198–204. https://doi.org/10.1016/j.neuron.2010.03.035.
Gabriel C, Gabriel S, Corthout E. The dielectric properties of biological tissues: I. Literature survey. Phys Med Biol 1996;41:2231–49. https://doi.org/10.1088/0031-9155/41/11/001.
Gabriel C, Peyman A, Grant EH. Electrical conductivity of tissue at frequencies below 1 MHz. Phys Med Biol 2009;54:4863. https://doi.org/10.1088/0031-9155/54/16/002.
Gomez-Tames J, Asai A, Hirata A. Significant group-level hotspots found in deep brain regions during transcranial direct current stimulation (tDCS): A computational analysis of electric fields. Clin Neurophysiol 2020;131:755–65. https://doi.org/10.1016/j.clinph.2019.11.018.
Guidetti M, Arlotti M, Bocci T, Bianchi AM, Parazzini M, Ferrucci R, et al. Electric Fields Induced in the Brain by Transcranial Electric Stimulation: A Review of In Vivo Recordings. Biomedicines 2022a;10:2333. https://doi.org/10.3390/biomedicines10102333.
Guidetti M, Bertini A, Pirone F, Sala G, Signorelli P, Ferrarese C, et al. Neuroprotection and Non-Invasive Brain Stimulation: Facts or Fiction? Int J Mol Sci 2022b;23:13775. https://doi.org/10.3390/IJMS232213775.
Guler S, Dannhauer M, Erem B, Macleod R, Tucker D, Turovets S, et al. Optimization of focality and direction in dense electrode array transcranial direct current stimulation (tDCS). J Neural Eng 2016:13. https://doi.org/10.1088/1741-2560/13/3/036020.
Holstege G, Tan J, van Ham JJ, Graveland GA. Anatomical observations on the afferent projections to the retractor bulbi motoneuronal cell group and other pathways possibly related to the blink reflex in the cat. Brain Res 1986;374:321–34. https://doi.org/10.1016/0006-8993(86)90426-9.
Huang Y, Parra LC. Can transcranial electric stimulation with multiple electrodes reach deep targets? Brain Stimul 2019;12:30–40. https://doi.org/10.1016/j.brs.2018.09.010.
Huang Y, Thomas C, Datta A. Optimized Transcutaneous Spinal Cord Direct Current Stimulation using Multiple Electrodes from 3/9/7 System. vol. 2019. Institute of Electrical and Electronics Engineers Inc.; 2019. https://doi.org/10.1109/EMBC.2019.8856689.
Im C-H, Park J-H, Shim M, Chang WH, Kim Y-H. Evaluation of local electric fields generated by transcranial direct current stimulation with an extracephalic reference electrode based on realistic 3D body modeling. Phys Med Biol 2012;57:2137. https://doi.org/10.1088/0031-9155/57/8/2137.
Kennelly KD. Clinical neurophysiology of cranial nerve disorders. Handb Clin Neurol 2019;161:327–42. https://doi.org/10.1016/B978-0-444-64142-7.00058-8.
Khan A, Antonakakis M, Vogenauer N, Haueisen J, Wolters CH. Individually optimized multi-channel tDCS for targeting somatosensory cortex. Clin Neurophysiol 2022;134:9–26. https://doi.org/10.1016/J.CLINPH.2021.10.016.
Khorrampanah M, Seyedarabi H, Daneshvar S, Farhoudi M. Optimization of montages and electric currents in tDCS. Comput Biol Med 2020;125. https://doi.org/10.1016/J.COMPBIOMED.2020.103998 103998.
Kimura J. Electrically elicited blink reflex in diagnosis of multiple sclerosis. Review of 260 patients over a seven-year period. Brain. J Neurol 1975;98:413–26. https://doi.org/10.1093/BRAIN/98.3.413.
Kimura J. Disorder of interneurons in parkinsonism: The orbicularis oculi reflex to paired stimuli1. Brain 1973;96:87–96. https://doi.org/10.1093/brain/96.1.87.
Kimura J, Daube J, Burke D, Hallett M, Cruccu G, Ongerboer de Visser BW, et al. Human reflexes and late responses. Report of an IFCN committee. Electroencephalogr Clin Neurophysiol 1994;90:393–403. https://doi.org/10.1016/0013-4694(94)90131-7.
Kimura J, Lyon LW. Orbicularis oculi reflex in the Wallenberg syndrome: alteration of the late reflex by lesions of the spinal tract and nucleus of the trigeminal nerve. J Neurol Neurosurg Psychiatry 1972;35:228–33. https://doi.org/10.1136/JNNP.35.2.228.
Kronberg G, Rahman A, Sharma M, Bikson M, Parra LC. Direct current stimulation boosts hebbian plasticity in vitro. Brain Stimul 2020;13:287–301. https://doi.org/10.1016/j.brs.2019.10.014.
Kugelberg E. Facial reflexes. Brain J Neurol 1952;75:385–96. https://doi.org/10.1093/BRAIN/75.3.385.
Kuo HI, Bikson M, Datta A, Minhas P, Paulus W, Kuo MF, et al. Comparing Cortical Plasticity Induced by Conventional and High-Definition 4 × 1 Ring tDCS: A Neurophysiological Study. Brain Stimul 2013;6:644–8. https://doi.org/10.1016/J.BRS.2012.09.010.
Kuypers HGJM. Corticobulbar connexions to the pons and lower brain-stem in manan anatomical study. Brain 1958;81:364–88. https://doi.org/10.1093/BRAIN/81.3.364.
Lamy J-C, Boakye M. BDNF Val66Met polymorphism alters spinal DC stimulation-induced plasticity in humans. J Neurophysiol 2013;110:109–16. https://doi.org/10.1152/jn.00116.2013.
Lang N, Siebner HR, Chadaide Z, Boros K, Nitsche MA, Rothwell JC, et al. Bidirectional Modulation of Primary Visual Cortex Excitability: A Combined tDCS and rTMS Study. Invest Ophthalmol Vis Sci 2007;48:5782–7. https://doi.org/10.1167/IOVS.07-0706.

Lefaucheur J-P, Antal A, Ayache SS, Benninger DH, Brunelin J, Cogiamanian F, et al. Evidence-based guidelines on the therapeutic use of transcranial direct current stimulation (tDCS). Clin Neurophysiol 2017;128:56–92. https://doi.org/10.1016/j.clinph.2016.10.087.

Manca D, Muoz E, Pastor P, Valldeoriola F, Valls-Solé J. Enhanced gain of blink reflex responses to ipsilateral supraorbital nerve afferent inputs in patients with facial nerve palsy. Clin Neurophysiol 2001;112:153–6. https://doi.org/10.1016/S1388-2457(00)00516-2.

Manto M, Argyropoulos GPD, Bocci T, Celnik PA, Corben LA, Guidetti M, et al. Consensus Paper: Novel Directions and Next Steps of Non-invasive Brain Stimulation of the Cerebellum in Health and Disease. Cerebellum Lond Engl 2021. https://doi.org/10.1007/s12311-021-01344-6.

Mao JB, Evinger C. Long-Term Potentiation of the Human Blink Reflex. J Neurosci 2001;21:RC151. https://doi.org/10.1523/JNEUROSCI.21-12-J0002.2001.

Mendonca ME, Santana MB, Baptista AF, Datta A, Bikson M, Fregni F, et al. Transcranial DC Stimulation in Fibromyalgia: Optimized Cortical Target Supported by High-Resolution Computational Models. J Pain 2011;12:610–7. https://doi.org/10.1016/J.JPAIN.2010.12.015.

Mesquita PHC, Franchini E, Romano-Silva MA, Lage GM, Albuquerque MR. Transcranial Direct Current Stimulation: No Effect on Aerobic Performance, Heart Rate, or Rating of Perceived Exertion in a Progressive Taekwondo-Specific Test. Int J Sports Physiol Perform 2020;15:958–63. https://doi.org/10.1123/IJSPP.2019-0410.

Mishra P, Pandey CM, Singh U, Gupta A, Sahu C, Keshri A. Descriptive Statistics and Normality Tests for Statistical Data. Ann Card Anaesth 2019;22:67. https://doi.org/10.4103/ACA.ACA_157_18.

Nitsche MA, Cohen LG, Wassermann EM, Priori A, Lang N, Antal A, et al. Transcranial direct current stimulation: State of the art 2008;1:2008.

Nitsche MA, Paulus W. Excitability changes induced in the human motor cortex by weak transcranial direct current stimulation. J Physiol 2000;527:633–9. https://doi.org/10.1111/j.1469-7793.2000.t01-1-00633.x.

Noetscher GM, Yanamadala J, Makarov SN, Pascual-Leone A. Comparison of cephalic and extracephalic montages for transcranial direct current stimulation-a numerical study. IEEE Trans Biomed Eng 2014;61:2488–98. https://doi.org/10.1109/TBME.2014.2322774.

Nonnekes J, Arrogi A, Munneke MAM, Van Asseldonk EHF, Nijhuis LBO, Geurts AC, et al. Subcortical Structures in Humans Can Be Facilitated by Transcranial Direct Current Stimulation. PLoS One 2014;9:e107731.

Ongerboer De Visser BW, Goor C. Jaw reflexes and masseter electromyograms in mesencephalic and pontine lesions: an electrodiagnostic study. J Neurol Neurosurg Psychiatry 1976;39:90–2. https://doi.org/10.1136/JNNP.39.1.90.

Ongerboer De Visser BW, Kuypers HGJM. Late blink reflex changes in lateral medullary lesions. An electrophysiological and neuro-anatomical study of Wallenberg's Syndrome. Brain. J Neurol 1978;101:285–94. https://doi.org/10.1093/BRAIN/101.2.285.

Opitz A, Paulus W, Will S, Antunes A, Thielscher A. Determinants of the electric field during transcranial direct current stimulation. Neuroimage 2015;109:140–50. https://doi.org/10.1016/j.neuroimage.2015.01.033.

Parazzini M, Fiocchi S, Ravazzani P. Electric field and current density distribution in an anatomical head model during transcranial direct current stimulation for tinnitus treatment. Bioelectromagnetics 2012;33:476–87.

Parazzini M, Fiocchi S, Rossi E, Paglialonga A, Ravazzani P. Transcranial direct current stimulation: Estimation of the electric field and of the current density in an anatomical human head model. IEEE Trans Biomed Eng 2011;58:1773–80. https://doi.org/10.1109/TBME.2011.2116019.

Parazzini M, Rossi E, Ferrucci R, Liorni I, Priori A, Ravazzani P. Modelling the electric field and the current density generated by cerebellar transcranial DC stimulation in humans. Clin Neurophysiol 2014;125:577–84. https://doi.org/10.1016/j.clinph.2013.09.039.

Parazzini M, Rossi E, Rossi L, Priori A, Ravazzani P, Cogiamanian F, et al. Evaluation of the current density in the brainstem during transcranial direct current stimulation with extra-cephalic reference electrode. Clin Neurophysiol 2013;124:1039–40. https://doi.org/10.1016/J.CLINPH.2012.09.021.

Park JH, Hong SB, Kim DW, Suh M, Im CH. A novel array-type transcranial direct current stimulation (tDCS) system for accurate focusing on targeted brain areas. IEEE Trans Magn 2011;47:882–5. https://doi.org/10.1109/TMAG.2010.2072987.

Pellegrini M, Zoghi M, Jaberzadeh S. The effects of transcranial direct current stimulation on corticospinal and cortico-cortical excitability and response variability: Conventional versus high-definition montages. Neurosci Res 2021;166:12–25. https://doi.org/10.1016/j.neures.2020.06.002.

Peterchev AV, Wagner TA, Miranda PC, Nitsche MA, Paulus W, Lisanby SH, et al. Fundamentals of transcranial electric and magnetic stimulation dose: Definition, selection, and reporting practices. Brain Stimul 2012;5:435–53. https://doi.org/10.1016/j.brs.2011.10.001.

Priori A, Maiorana N, Dini M, Guidetti M, Marceglia S, Ferrucci R. Adaptive deep brain stimulation (aDBS). Int Rev Neurobiol 2021;159:111–27. https://doi.org/10.1016/bs.irn.2021.06.006.

Rashed EA, Gomez-Tames J, Hirata A. End-to-end semantic segmentation of personalized deep brain structures for non-invasive brain stimulation. Neural Netw 2020;125:233–44. https://doi.org/10.1016/j.neunet.2020.02.006.

Reato D, Rahman A, Bikson M, Parra LC. Low-intensity electrical stimulation affects network dynamics by modulating population rate and spike timing. J Neurosci 2010;30:15067–79. https://doi.org/10.1523/JNEUROSCI.2059-10.2010.

Roos D, Biermann L, Jarczok TA, Bender S. Local Differences in Cortical Excitability – A Systematic Mapping Study of the TMS-Evoked N100 Component. Front Neurosci 2021;15.

Ruffini G, Fox MD, Ripolles O, Miranda PC, Pascual-Leone A. Optimization of multifocal transcranial current stimulation for weighted cortical pattern targeting from realistic modeling of electric fields. Neuroimage 2014;89:216–25. https://doi.org/10.1016/J.NEUROIMAGE.2013.12.002.

Sadleir RJ, Vannorsdall TD, Schretlen DJ, Gordon B. Target optimization in transcranial direct current stimulation. Front Psych 2012;3:90. https://doi.org/10.3389/FPSYT.2012.00090/BIBTEX.

Schoenen J. Exteroceptive suppression of temporalis muscle activity: methodological and physiological aspects. Cephalalgia Int J Headache 1993;13:3–10. https://doi.org/10.1046/J.1468-2982.1993.1301003.X.

Shahani BT, Young RR. Human orbicularis oculi reflexes. Neurology 1972;22:149–54. https://doi.org/10.1212/WNL.22.2.149.

Siebner HR, Lang N, Rizzo V, Nitsche MA, Paulus W, Lemon RN, et al. Preconditioning of Low-Frequency Repetitive Transcranial Magnetic Stimulation with Transcranial Direct Current Stimulation: Evidence for Homeostatic Plasticity in the Human Motor Cortex. J Neurosci 2004;24:3379–85. https://doi.org/10.1523/JNEUROSCI.5316-03.2004.

Thomas C, Huang Y, Faria PC, Datta A. High-resolution head model of transcranial direct current stimulation: A labeling analysis. Proc. Annu. Int. Conf. IEEE Eng. Med. Biol. Soc. EMBS, Institute of Electrical and Electronics Engineers Inc. 2019:6442–5. https://doi.org/10.1109/EMBC.2019.8857181.

Wagner S, Burger M, Wolters CH. An optimization approach for well-targeted transcranial direct current stimulation. SIAM J Appl Math 2016;76:2154–74. https://doi.org/10.1137/15M1026481.

Woods AJ, Antal A, Bikson M, Boggio PS, Brunoni AR, Celnik P, et al. A technical guide to tDCS, and related non-invasive brain stimulation tools. Clin Neurophysiol 2016;127:1031–48. https://doi.org/10.1016/j.clinph.2015.11.012.